Journal of Magnetic Resonance **140,** 460–470 (1999)
Article ID jmre.1999.1854, available online at http://www.idealibrary.com on IDEAL®

Combined Reduced 4D ^{13}C Exchange and ^{1}H Spin Diffusion Experiment for Determining the Length Scale of Dynamic Heterogeneities

U. Tracht, M. Wilhelm, A. Heuer, and H. W. Spiess

MPI für Polymerforschung, Ackermannweg 10, D-55128 Mainz, Germany

Received February 22, 1999; revised June 16, 1999

A multidimensional static solid-state NMR experiment is described that combines ^{13}C exchange sequences with ^{1}H spin diffusion. It realizes a spatial correlation of different reorientation rates. By means of this experiment the length scale of dynamic heterogeneities can be measured directly. The pulse sequence and phase cycle as well as the experimental setup procedure and data analysis are described in detail. It complements the previous letter on this subject where a brief report of the main results were presented (U. Tracht *et al.,* 1998, *Phys. Rev. Lett.* 81, 2727). Application of this experiment to an amorphous polymer in the supercooled state yields a length scale of immobile regions of about 3 *nm*. © 1999 Academic Press

INTRODUCTION

Amorphous systems in the glass transition range exhibit characteristic dynamic properties regardless of their chemical structure (*1, 2*); e.g., the α-relaxation is highly nonexponential. A number of studies on different fragile glass formers (*3–12*) has shown that the nonexponential α-relaxation can be attributed to the existence of dynamic heterogeneities; i.e., the macroscopically nonexponential relaxation functions are due to a superposition of different relaxation rates. Dynamic heterogeneities can be characterized by the time scale of fluctuations of relaxation rates within the rate distribution and by the spatial extension of temporary clusters of slow molecules; see Fig. 1. The question whether the glass transition is connected with a characteristic length scale is an important aspect of the theoretical understanding of the freezing process in supercooled liquids. Several theories postulate the divergence of a characteristic length scale at the glass transition. The length scale of dynamic heterogeneities can, for example, be related to the size of the cooperatively rearranging regions introduced by Adam and Gibbs (*13*). Different experimental approaches have been developed to determine a characteristic length scale of the glass transition but apart from two new types of experiments (*14, 15*) these techniques involve external perturbations of the investigated dynamics (*16–18, 8*) or rely on model assumptions about the relaxation mechanism for relating experimental data to a cooperativity length (*19, 20*). Computer simulations of different model glasses have revealed the significance of a cooperativity length for the dynamics of, e.g., Ising spin glasses (*21, 22*), lattice-gas models (*23*), and Lennard–Jones liquids (*24*).

Among the experimental techniques used to study relaxation processes in glass formers and in particular dynamic heterogeneities multidimensional solid-state NMR has become an indispensable tool (*5, 9, 10, 25, 26*). The temporal evolution of selected relaxation rates has already been analyzed extensively by reduced four-dimensional solid-state exchange NMR (4D echo experiment) (*5, 9, 10, 27–31*). Application of this technique to a variety of polymers and low-molar glass formers has shown that slow molecules change their rate after only one reorientation process. The determination of the characteristic length scale of dynamic heterogeneities is much more complicated because it requires spatially resolved characterization of dynamic properties in single component systems which do not exhibit chemical contrast. In a recent publication (*15*) results from a new multidimensional NMR experiment (4D-cross polarization (CP) echo experiment) that allows direct determination of the length scale of dynamic heterogeneities have been presented.

The present contribution is to focus on the complex experimental procedure as well as the data analysis to determine the length scale of the dynamic heterogeneities. First of all, the basic idea of the 4D echo and the 4D-CP echo experiment is described; in the following paragraphs the pulse sequence and the experimental setup of the 4D-CP echo experiment are discussed and finally a theoretical model is presented by which means a quantitative analysis of the experimental data is performed. Note that we apply this technique to chemical homogeneous systems rather than the simpler case of blends or block-copolymers where already the structural heterogeneities imply trivial dynamic heterogeneities.

4D-CP ECHO EXPERIMENT

The experiment developed for the determination of the length scale of dynamic heterogeneities is an extension of the

1090-7807/99 $30.00

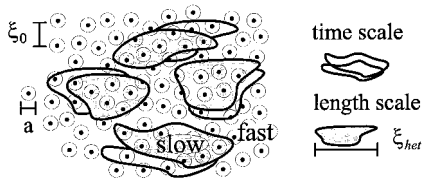

FIG. 1. Schematic representation of the time scale and the length scale ξ_{het} of dynamic heterogeneities. The time scale is related to the temporal fluctuations in the sense that a specified segment may switch between a fast and a slow state. Furthermore, the positions of the individual ^{13}C spins are indicated. The length scales ξ_0 and a are significant for the quantitative analysis of the 4D-CP echo experiment and are explained in Sections 2 and 4, respectively.

4D exchange experiments used to measure the temporal evolution of selected reorientation rates (*5, 9*). In the original version (*5*) just one of the evolution times of the 4D experiment was incremented so that full two-dimensional ^{13}C spectra were recorded in order to achieve spectral resolution of different chemical sites in samples with ^{13}C in natural abundance. Later, using samples with selective isotopic labeling it was sufficient to record only echo-signals (*9*). Since much less time is required for recording an echo rather than a full 2D data set, systematic variation of the intermediate mixing time was possible (4D echo experiment). By combining the latter experiment with ^{1}H spin diffusion spatial information is accessible. The basic principle of both techniques is sketched in Fig. 2 for the case of a bimodal distribution with rates k_{slow} and k_{fast}. The first part of the 4D echo as well as the 4D-CP echo experiment acts as a filter that leaves magnetization only on immobile molecules or segments. During the variable waiting time t_{m2} two different equilibration processes may take place. On the one hand the mobility of initially slow segments may change (Fig. 2a). The 4D echo experiment monitors such fluctuations of rates by finally selecting the components that are still immobile after the waiting time. On the other hand spatial redistribution of magnetization from the immobile toward the mobile regions may occur (Fig. 2b). Under the assumption that the rate distribution is static on the time scale of the experiment the 4D-CP echo experiment measures the amount of magnetization that is still on the initially selected immobile spins after the equilibration time. The final echo height as a function of the waiting time corresponds to a four-time correlation function in the case of the 4D echo experiment whereas the 4D-CP echo experiment achieves four-time correlation together with a spatial correlation. The experimental realization of the principle illustrated in Fig. 2 is described in the following.

Pulse sequences and phase cycles are presented for the case of static ^{13}C-CP measurements. The 4D echo experiment has mostly been applied to ^{2}H so far (*10, 27, 29, 30, 32, 33*). The pulse sequences of the ^{13}C 4D echo and the 4D-CP echo experiments are shown in Figs. 3a and 3b, respectively. The exchange sequences are based on the orientation dependence of the resonance frequencies. Dynamic selection is achieved by 2D echo sequences as described previously (*9, 34*). Only magnetization from segments that have not changed their orientations during the filter time t_{m0} contribute to the final echo given by $\langle\cos((\omega_1 - \omega_2)t_p)\rangle \approx \langle\cos(\omega_1 t_p)\cos(\omega_2 t_p)\rangle$. The geometric sensitivity of this filter is determined by the product of the evolution time t_p and the chemical shift anisotropy δ. The smaller the reorientation angle to be probed the larger $t_p\delta$ has to be in order to detect single reorientation processes. The 4D echo experiment consists of two 2D echo sequences with filter times t_{m0} separated by the variable waiting time t_{m2}; see Fig. 3a. By appropriately choosing the pulse phases (Table 1a) the four-time correlation function

$$F_4(t_{m2}) = \langle\cos((\omega_1 - \omega_2)t_p)\cos(\omega_3 t_p)\cos(\omega_4 t_p)\rangle \qquad [1]$$

is measured. Quantitative analysis of this function is possible in terms of a rate memory parameter Q (*35*). Q can be interpreted as the number of reorientations that a selected slow segment performs before it changes its rate. For all organic fragile glass forming systems studied so far fast fluctuations of

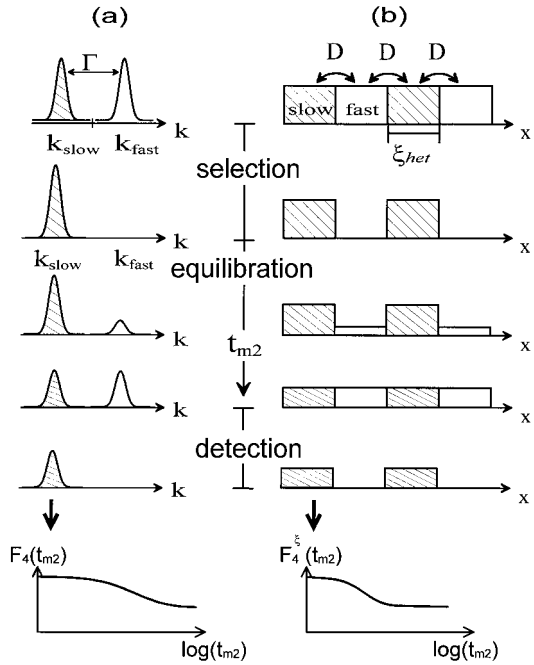

FIG. 2. Schematic representation of the 4D (left) and the 4D-CP (right) echo experiments for a bimodal reorientation rate distribution. In the first part of both experiments immobile segments with rate k_{slow} are selected. Equilibration of the distribution of magnetization during the variable waiting time t_{m2} may take place either via changes of the rates of selected segments with exchange rate Γ (4D echo experiment) or via spatial distribution of magnetization with spin diffusion constant D from the immobile toward the mobile segments (4D-CP echo experiment). Finally, the same filter as in the beginning of the experiments is applied again; thus, by the 4D echo experiment those components that have not changed their rates during t_{m2} and in the 4D-CP echo experiment the amount of magnetization that is still in the immobile regions are detected. The resulting echo decay curves $F_4(t_{m2})$ and $F_4^{\xi}(t_{m2})$ contain information about the exchange rate Γ and the length scale of dynamic heterogeneities ξ_{het}, respectively.

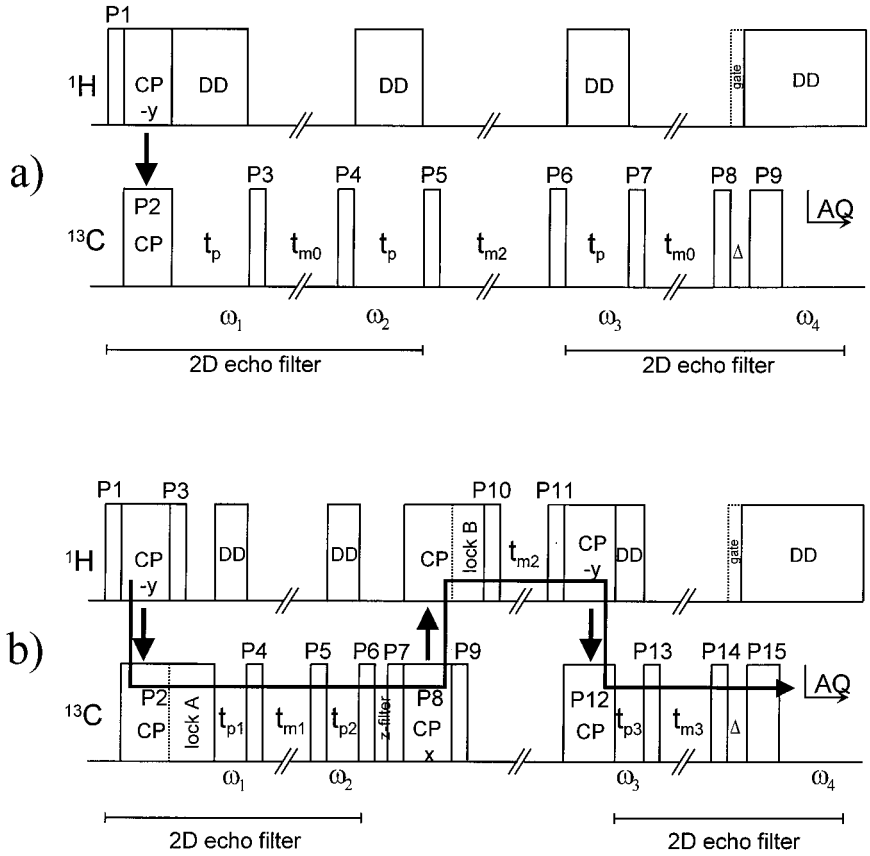

FIG. 3. Pulse sequences for the 4D and the 4D-CP echo experiments. ^{13}C magnetization is created via cross polarization. Heteronuclear continuous wave decoupling is applied during all evolution and detection times. Gated decoupling during the Hahn echo delay can be applied in order to suppress signal contributions from aliphatic carbon atoms. Both pulse sequences consist of two 2D echo filters separated by a waiting time t_{m2}, thereby realizing a correlation of segmental orientations at four times. As compared to the 4D echo experiment the 4D-CP echo experiment is extended by two cross-polarization steps before and after t_{m2} in order to enable spin diffusion between regions of slow and fast segments. In both experiments the echo height is measured as a function of t_{m2} for fixed evolution times t_p and filter times t_{m0} or t_{m1} and t_{m3}, respectively.

selected rates corresponding to rate memory parameters Q on the order of 1 have been found (*9, 10, 27–29, 31*). The underlying rate distributions typically covered 2–4 orders of magnitude. Since the NMR echo experiments are sensitive to the α-relaxation these exchange processes directly contain information about the nature of the main relaxation of the glass transition.

In order to obtain information about length scales in dynamically heterogeneous systems solid state NMR often exploits spin diffusion (*25*). In contrast to ^{1}H spin diffusion experiments on multicomponent systems with largely different mobilities, standard selection techniques are not applicable to determine the length scale ξ_{het} of dynamic heterogeneities at the glass transition in chemically homogeneous systems. Dynamic selection is easily feasible by ^{13}C 2D echo filters but ^{13}C spin diffusion can often not be exploited in such systems because for partly ^{13}C-labeled samples like the one used in the present investigation ^{13}C spin diffusion is usually negligible on the typical time scale of the experiment. Of course, this is an essential requirement for the 4D echo experiment to be sensitive to rate exchange, treating the effects of spin diffusion only as a small perturbation. For designing an experiment to measure ξ_{het} we exploit that ^{1}H spin diffusion is much faster than ^{13}C spin diffusion because of the higher gyromagnetic ratio, higher spin density, and natural abundance. Therefore the 4D-CP echo experiment combines ^{13}C 2D echo filters with ^{1}H spin diffusion in order to achieve four-time as well as spatial correlation. The signal $F_4^{\xi}(t_{m2})$ that is recorded at the end of the pulse sequence and which is equivalent to the integral magnetization of the immobile domains is given by

$$F_4^{\xi}(t_{m2}) \propto \frac{1}{(4\pi D t_{m2})^{3/2}} \sum_{i,j} \cos((\omega_1^i - \omega_2^i)t_p) \exp\left(-\frac{(\mathbf{r}_i(0) - \mathbf{r}_j(t_{m2}))^2}{4Dt_{m2}}\right) \cos(\omega_3^j t_p)\cos(\omega_4^j t_p). \quad [2]$$

D denotes the spin diffusion coefficient and the sum refers to

TABLE 1
Phase Cycles for the Echo Experiments

(a) 4D

1H-M	++++++++	++++++++	++++++++	++++++++
P1 $\pi/2$	02020202	02020202	02020202	02020202
P2	00112233	00112233	00112233	00112233
13C-M	02132031	02132031	02132031	02132031
P3 $\pi/2$	13203102	31021320	20310213	02132031
	cos ω1t1	cos ω1t1	sin ω1t1	sin ω1t1
13C-M	++++++++	−−−−−−−−	++++++++	−−−−−−−−
P4 $\pi/2$	31021320	13203102	20310213	02132031
13C-M	02132031	02132031	31021320	31021320
P5 $\pi/2$	11223300	11223300	11223300	11223300
	cos ω2t2	cos ω2t2	sin ω2t2	sin ω2t2
13C-M	+−+−+−+−	+−+−+−+−	+−+−+−+−	+−+−+−+−
P6 $\pi/2$	02132031	02132031	02132031	02132031
13C-M	11223300	11223300	11223300	11223300
P7 $\pi/2$	20310213	02132031	20310213	02132031
	cos ω3t3	cos ω3t3	cos ω3t3	cos ω3t3
13C-M	+−+−+−+−	−+−+−+−+	+−+−+−+−	−+−+−+−+
P8 $\pi/2$	02132031	20310213	02132031	20310213
13C-M	11223300	11223300	11223300	11223300
P9	13203102	13203102	13203102	13203102
13C-M	11223300	11223300	11223300	11223300

(b) 4D-CP

1H-M	++++++++	++++++++	++++++++	++++++++
P1 $\pi/2$	02020202	02020202	02020202	02020202
P2 (lock)	00112233	00112233	00112233	00112233
P3 $\pi/2$	20202020	20202020	20202020	20202020
13C-M	02132031	02132031	02132031	02132031
P4 $\pi/2$	13203102	31021320	20310213	02132031
	cos ω1t1	cos ω1t1	sin ω1t1	sin ω1t1
13C-M	++++++++	−−−−−−−−	++++++++	−−−−−−−−
P5 $\pi/2$	31021320	13203102	20310213	02132031
13C-M	02132031	02132031	31021320	31021320
P6 $\pi/2$	11223300	11223300	11223300	11223300
13C-M	+−+−+−+−	+−+−+−+−	+−+−+−+−	+−+−+−+−
	cos ω2t2	cos ω2t2	sin ω2t2	sin ω2t2
P7 $\pi/2$	33333333	33333333	33333333	33333333
13C-M	02020202	02020202	02020202	02020202
13C lock	00000000	00000000	00000000	00000000
P8 (lock)	00112233	00112233	00112233	00112233
P9 $\pi/2$	13131313	13131313	13131313	13131313
13C-M	++++++++	++++++++	++++++++	++++++++
1H-M	02132031	02132031	02132031	02132031
P10 $\pi/2$	11223300	11223300	11223300	11223300
1H-M	+−+−+−+−	+−+−+−+−	+−+−+−+−	+−+−+−+−
P11 $\pi/2$	00000000	22222222	00000000	22222222
1H-M	13131313	13131313	13131313	13131313
1H lock	33333333	33333333	33333333	33333333
P12 (lock)	00112233	00112233	00112233	00112233
13C-M	02132031	20310213	02132031	20310213
P13 $\pi/2$	11223300	11223300	11223300	11223300
	cos ω3t3	cos ω3t3	cos ω3t3	cos ω3t3
13C-M	+−+−+−+−	−+−+−+−+	+−+−+−+−	−+−+−+−+
P14 $\pi/2$	11111111	22222222	33333333	00000000
P15 π	00002222	11113333	00002222	11113333
13C-M	20202020	13131313	02020202	31313131

Note. The numbers $n = 0, 1, 2, 3$ correspond to $x, y, -x, -y$ pulse phases. + and − stand for $+z$ and $-z$ magnetization, respectively. Since spin-$\frac{1}{2}$ transitions are considered the effect of the pulses can be visualized in the vector picture. The direction of rotation of the magnetization is determined according to the left-handed convention (*25*), e.g., $+z$ magnetization is rotated to the $(n + 1)$ axis by a pulse with phase n. The pulse phases are adjusted such that the first 2D filter sequence (pulses P1 to P4) generates the $\cos(\omega_1 t_p)\cos(\omega_2 t_p) + \sin(\omega_1 t_p)\sin(\omega_2 t_p)$ signal and the final filter (pulses P6 to P9 in the 4D echo experiment and P12 to P15 in the 4D-CP echo experiment) yields only the $\cos(\omega_3 t_p)\cos(\omega_4 t_p)$ signal. Contributions from magnetization that has built up during the mixing times due to spin lattice relaxation are eliminated by storing alternately $+z$ and $-z$ magnetization. Furthermore CYCLOPS and the cross-polarization phase cycling are included.

all ^{13}C spins. This expression results from the solution of the three-dimensional diffusion equation for a point source (*36*). It is valid in the present form only if one assumes spin diffusion among ^{13}C spins. In reality D stands for the ^{1}H spin diffusion coefficient and a full description of the experiment is more complicated as will be discussed below. The pulse sequence used to measure $F_4^{\xi}(t_{m2})$ is given in Fig. 3b. In principle the evolution times in the beginning, t_{p1}, t_{p2}, and at the end, t_{p3}, can all be chosen differently. This is exploited, e.g., for recording the reference data; see below. In the actual application of the sequence to determine ξ_{het}, all three are taken to be equal to t_p. After the first 2D sequence with filter time t_{m0} the selected magnetization is transferred to protons surrounding the ^{13}C spins via cross polarization. At the end of the waiting time t_{m2} the ^{1}H magnetization is transferred back to ^{13}C. Finally another 2D echo filter selects the magnetization that is left in immobile regions. The phase cycle as described in Table 1b in combination with additional filter steps (lock A, lock B, z filter) guarantees that only the desired magnetization contributes to the final echo signal. During the lock pulses lock A and lock B residual transverse magnetization on the respective other nuclei decays under homonuclear dipolar coupling and hence does not add to the magnetization created by cross polarization. The z filter preceding the crosspolarization from ^{13}C to ^{1}H makes it possible to have a constant phase for the ^{13}C CP lock pulse and additionally suppresses multiple quantum coherences or magnetization resulting from pulse imperfections. The efficiency of the phase cycle has been checked by performing the experiment with the second CP pulse on the ^{13}C channel omitted. No signal resulting just from ^{1}H single pulse excitation could be detected.

The function F_4^{ξ} measured by the 4D-CP echo experiment is more complicated than standard spin diffusion curves because of the two cross polarization steps before and after t_{m2}. Yet, this experiment has the advantage that it can be interpreted without specific assumptions about the diffusion coefficient. In principle, the length scale ξ_{het} of dynamic heterogeneities can be obtained from a spin diffusion experiment by solving the diffusion equation under the assumption of some reasonable value for the diffusion coefficient D inferred from similar systems (*25, 37*). Values for D have been determined for model systems with well-defined domain sizes and topologies (*37, 38*). These values cannot be generalized to the 4D-CP echo data because the effective diffusion coefficient is on the one hand influenced by the amount of magnetization transferred during the CP and spin-lock times that is hard to estimate because each lock pulse scales the dipolar coupling by a factor of -0.5 (*39*). On the other hand D may depend on the mobility of the selected component. The 4D-CP echo experiment has the advantage that the next nearest neighbor distance ξ_0 of labeled ^{13}C atoms can be used as an internal reference. The principle sketched in Fig. 2b is only valid for complete transfer of magnetization from protons to ^{13}C by the cross polarization at the end of the spin diffusion time t_{m2}. In reality, only magnetization from carbons close enough to ^{13}C atoms is transferred; the rest is lost to the proton bath. This means that even without any dynamic selection the spin diffusion curve decays with increasing t_{m2} due to distribution of magnetization over the proton bath. Equilibrium is reached when the magnetization has diffused to the nearest ^{13}C atom over an average distance ξ_0. The time scale of this decay of F_4^{ξ} is a measure of the length scale ξ_0 whereas the amplitude of the decay is a measure of the distance over which ^{1}H magnetization can be transferred to ^{13}C atoms via cross polarization. If the two length scales ξ_0 and ξ_{het} are significantly different the spin diffusion curve shows a two-step decay with the first decay corresponding to diffusion on the length scale ξ_0 and the second decay corresponding to diffusion over the distance ξ_{het} (*15*). The first diffusion process can be measured separately by performing the 4D-CP echo experiment without dynamic selection. Since the corresponding distance ξ_0 is known from the degree of isotopic enrichment the effective diffusion coefficient can be determined from this reference experiment. Moreover, by comparing the results of the experiments with and without selection of immobile components the length scale ξ_{het} can be determined without any assumptions about the diffusion coefficient, the topology of the mobility distribution, or the influence of the cross-polarization sequences on the spin diffusion.

EXPERIMENTAL

A polyvinyl acetate sample selectively ^{13}C-labeled at the carbonyl position has been studied. The carbonyl site has been shown to be a sensor of main chain reorientation (*40*). The isotopic enrichment amounts to 40% which corresponds to an average distance of ^{13}C atoms of $\xi_0 = 0.7$ nm. The chemical shift principal axes values are $\sigma_{xx} = 114 \pm 3$ ppm, $\sigma_{yy} = 138 \pm 3$ ppm, and $\sigma_{zz} = 260 \pm 3$ ppm corresponding to an anisotropy parameter of $\delta = 90$ ppm ($\triangleq 2\pi \cdot 6.8$ kHz at $B_0 = 7.05$ T) and an asymmetry parameter of $\eta = 0.27$. The glass transition as determined by DSC (heating rate 10K/min) is $T_g^{DSC} = 305$ K. Relevant relaxation times are $T_1(^{1}H) = 2.9$ s, $T_1(^{13}C) = 30$ s, $T_{CH} = 0.3$ ms, $T_{1\rho}(^{1}H) = 55$ ms, and $T_2^*(^{1}H) = 14$ μs. The sample has been dried in vacuum for several hours and annealed prior to sealing it in a glass tube under vacuum. The experiments have been performed on a Bruker MSL 300 spectrometer operating at ^{1}H and ^{13}C resonance frequencies of 300.13 and 75.47 MHz, respectively. A commercial Bruker static double resonance probe has been used. Data were acquired at $T = 315$ K $= T_g^{DSC} + 10$ K. The temperature has been chosen such that on the one hand the correlation times are sufficiently long that molecular dynamics during evolution and detection periods can be neglected and cross polarization is efficient. On the other hand the correlation times are short compared to T_1 relaxation and ^{13}C spin diffusion times.

The most important acquisition parameters are given in Table 2 and will be discussed in the following. The delays lock

TABLE 2
Acquisition Parameters Used in the 4D-CP Echo Experiment with the Pulse Sequence Given in Fig. 3

	Two-filter experiment	One-filter experiment
Lock A	500 μs	500 μs
Lock B	100 μs	100 μs
z filter	100 μs	100 μs
Δ	52 μs	52 μs
Gate	51 μs	51 μs
CP	0.8 ms	0.8 ms
t_{m1}; t_{m3}	3.5 ms; 3.5 ms	3.5 ms; 1 ms
$t_{p1,2}(t_p\delta)$; $t_{p3}(t_{p3}\delta)$	200 μs (8.5); 200 μs (8.5)	200 μs (8.5); 1 μs ($\rightarrow$0)
DW	2 μs	2 μs
Repetition delay	3 s	3 s
Accumulations per echo	9600	4800

Note. The choice of the different parameters is discussed in the text.

A, lock B, and z filter that are employed to support the phase cycle are chosen to be longer than the relevant T_2^* relaxation times but short enough to minimize the loss of magnetization via $T_{1\rho}$ relaxation during the lock pulse on the second channel. Gated decoupling during the Hahn echo delay Δ serves to suppress the signal from the aliphatic carbons present in natural abundance. The filter parameters t_p and $t_{m1} = t_{m3} = t_{m0}$ have been determined guided by results from 2D echo experiments. The evolution time t_p should be as short as possible in order to minimize loss of magnetization by T_2 relaxation but long enough to be sensitive to single reorientation processes. It has been set to 200 μs ($t_p\delta = 8.5$) which is the smallest value sensitive to reorientation angles $\alpha \gtrsim 10°$. The filter time t_{m0} determines what part of the rate distribution is selected. The two-time correlation function is well described by a stretched exponential $\exp[-(t/\tau_0)^{\beta_{KWW}}]$ with $\tau_0 = 16$ ms and $\beta_{KWW} = 0.45$; hence, a selection of about 60% is achieved by setting t_{m0} to 3.5 ms. Optimizing the cross-polarization time is very important for getting the experiment to work. It determines the total ^{13}C magnetization and the volume surrounding a ^{13}C spin to which magnetization is transferred during the CP pulse. Due to the limited efficiency of magnetization transfer each cross-polarization sequence results in a considerable loss of magnetization. For the reason explained in the following the contact times cannot be optimized to give maximum signal. A quantitative analysis of the 4D-CP echo experiment relies on the information about the time scale of diffusion over the distance ξ_0. Therefore the magnetization must still be closer to the initial ^{13}C spin at the end of the cross-polarization sequence. Only in this case does the spin diffusion on the length scale ξ_0 cause a measurable decay of the spin diffusion curve. Thus the contact time should be as short as possible while still yielding intense enough signal. The cross-polarization time has been optimized by performing the 4D-CP echo experiment without dynamic selection for different CP times. The resulting spin diffusion curves are displayed in Fig. 4. It is obvious that during a contact pulse of 1.6 ms an equilibration of magnetization has already taken place whereas the curves acquired with 0.8 and 0.5 ms CP pulses show the expected decay. Since there is no significant difference between the results for 0.8 and 0.5 ms contact times all experiments were performed with CP pulses of 0.8 ms because of the gain of signal as compared to a contact time of 0.5 ms.

There are two possibilities for measuring the curve without dynamic selection. In order to be directly comparable to the actual 4D-CP echo experiment it has to be recorded with the same pulse delays. Either both 2D echo filters are deactivated by setting all evolution times to $t_{p1,2} = t_{p3} = 1$ μs, hence reducing the geometric sensitivity, or the first filter may be retained, $t_{p1,2} = 200$ μs and $t_{p3} = 1$ μs. Ideally the resulting spin diffusion curves should be identical. Still differences between the two experiments are conceivable because the spin diffusion may be slowed down in the mobile regions due to a reduced homonuclear dipolar coupling. Furthermore in the mobile regions spin diffusion is superimposed by mass transport via reorientations of mobile segments. Finally the cross-polarization efficiency may also depend on the mobility. The experimental results (see Fig. 5) show that the spin diffusion curves from the two experiments are slightly different. Since the experiment with the first 2D echo sequence retained (one-filter experiment) and the full 4D-CP echo experiment (two-filter experiment) have identical initial conditions at the beginning of the spin diffusion time t_{m2} it is justified to assume a single effective spin diffusion coefficient for these two experiments, whereas the spin diffusion coefficient might be different in the case of the experiment without any dynamic selection for the reasons mentioned above. Therefore the one-filter experiment is used as a reference.

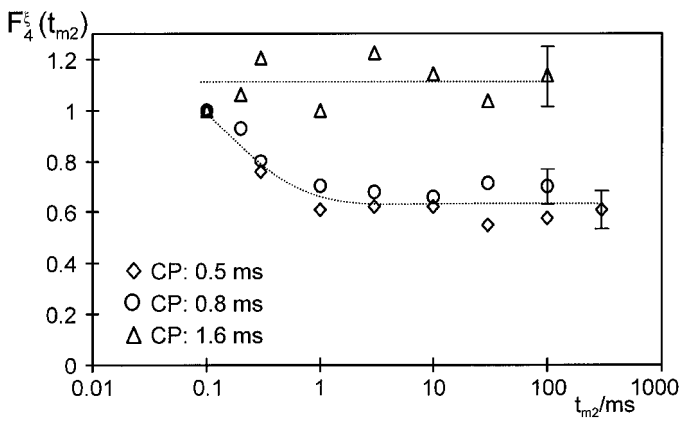

FIG. 4. Experimental data from the 4D-CP echo experiment without any dynamic selection ($t_p = 1$ μs, $t_{m0} = 1$ ms) for different cross-polarization contact times. The data show the equilibration of proton magnetization for long contact pulses. Dotted lines serve as a guide to the eye. The first data point has been normalized to unity, in all cases.

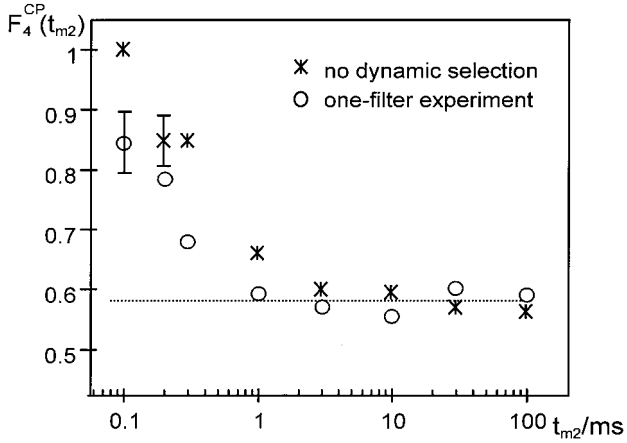

FIG. 5. Reference experiment measuring the spin diffusion process on the internal length scale ξ_0. Data from the experiment without any dynamic selection ($t_{p1,2} = t_{p3} = 1\ \mu$s) are compared to the one-filter experiment ($t_{p1,2} = 200\ \mu$s, $t_{p3} = 1\ \mu$s). Lines serve as a guide to the eye. The initial data point, obtained with no dynamic selection, has been normalized to unity.

ANALYSIS OF EXPERIMENTAL DATA

Results from the 4D echo experiment and the one-filter and two-filter 4D-CP echo experiments are shown in Fig. 6. Obviously, the spin diffusion curves F_4^{ξ} decay much faster than the four-time correlation function F_4 such that the requirement that the reorientation rate distribution is static on the time scale of the spin diffusion process is met. Also, the plateau value reached after the decay is completed is significantly lower for the two-filter experiment compared with that for the one-filter experiment. This shows that the experiment is capable of determining the length scale of the dynamic heterogeneities, ξ_{het}. The analysis of the data, necessary to extract ξ_{het}, is described in the following.

The model used to describe the 4D-CP echo experiment is based on the solution of the three-dimensional diffusion equation for a point source as expressed by Eq. [2]. For the present purpose the expression is rewritten as

$$F_4^{\xi}(t_{m2}) \propto \frac{1}{(4\pi D t_{m2})^{3/2}} \int \exp\left(-\frac{\mathbf{r}^2}{4Dt_{m2}}\right) \overline{\rho(\mathbf{r})}\, d\mathbf{r}, \qquad [3]$$

hence omitting the integration over all initial positions; see Appendix for a formal proof. $\overline{\rho(\mathbf{r})} = \delta(\mathbf{r}) + \rho_0(\mathbf{r})$ denotes the average density of immobile ^{13}C spins at position $\mathbf{r}$ relative to the initially selected ^{13}C spin. The delta function expresses the self-correlation term. $\rho_0(\mathbf{r})$ is the local density of ^{13}C spins. For the experiment without dynamic selection $\rho_0(\mathbf{r})$ is always given by the average density of ^{13}C atoms with distance ξ_0, $\rho_0(\mathbf{r}) = \xi_0^{-3}$. Otherwise $\rho_0(\mathbf{r})$ is lower because of the selection of only part of the ^{13}C spins. Equation [3] still neglects the effect of the magnetization transfer via crosspolarization.

A clustering of slow segments can be expressed by

$$\rho_0(\mathbf{r}) = \frac{1}{\xi_0^3}\left[p + (1-p)\exp\left(-\frac{2|\mathbf{r}|}{\xi_{het}}\right)\right], \qquad [4]$$

thus defining the correlation length ξ_{het}. This approach is analogous to the treatment of complex two component systems as described in (*37*) where the distribution of the selected component is modeled as clusters of extension ξ_{het} that are surrounded by regions with average density p/ξ_0^3 of the selected component. This means that close to the selected ^{13}C atom the probability of finding another immobile segment is high whereas for distances much longer than ξ_{het} one ends up with an average probability p. p is determined by the selected part of the rate distribution. It is equivalent to the final value of the four-time correlation function, $p = F_4(t_{m2} \to \infty) = F_4^{\infty}$; see also Fig. 1b. For the one-filter experiment one has $p = 1$. As

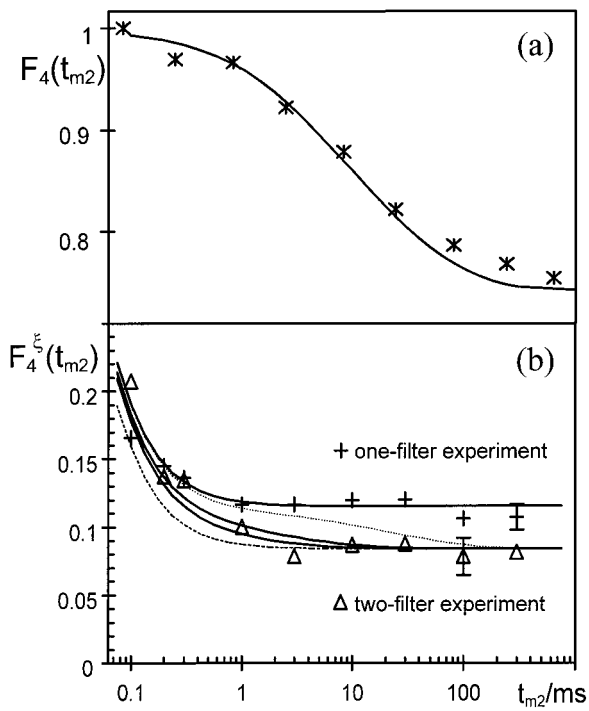

FIG. 6. Experimental data from the 4D and the 4D-CP echo experiment. (a) F_4 has been normalized to $F_4(t_{m2} = 0) = 1$. The solid line is the theoretical curve for a rate memory parameter $Q = 1$. (b) F_4^{ξ} from the one-filter (upper curve) and the two-filter (lower curve) 4D-CP echo experiments. Because of the poor signal-to-noise ratio echo heights from the 4D-CP echo experiments have been determined by fitting the echo signals to Gaussians. Experimental errors are indicated for the data points at longest mixing time only. The normalization is discussed in the text. The curves result from model calculations with $a = 0.1$ nm and $D = 0.42$ nm^2/ms as described in the text. Upper solid line, equilibration on the length scale ξ_0; lower dashed line, statistical distribution ($\xi_{het} = 0$) of different reorientation rates; lower solid lines, length scales ξ_{het} of 2 and 4 nm, respectively; lower dotted line, upper limit of experimentally accessible length scales corresponding to $\xi_{het} \approx 20$ nm.

already mentioned, details of the magnetization transfer and rate exchange processes have been neglected so far. These effects can be taken into account by the following model assumptions: (i) after the crosspolarization from carbons to protons the distribution of magnetization around the initial ^{13}C atom is given by a Gaussian with variance a^2; see also Fig. 1. The parameter a cannot be directly translated into a carbon–proton distance; (ii) The transfer of proton magnetization at $\mathbf{r}_H$ to a ^{13}C spin at $\mathbf{r}_C$ at the end of t_{m2} is proportional to $\exp(-(\mathbf{r}_H - \mathbf{r}_C)^2/2a^2)$; and (iii) the cluster of immobile segments surrounding a given spin disappears by exchange processes as expressed by F_4. The explicit calculation of F_4^ξ is straightforward but somewhat technical and is therefore given in the Appendix. Adjustable parameters for the model curves are D, a, and ξ_{het}. The model curves shown in Fig. 6 have been obtained with $a = 0.1$ nm and $D = 0.42$ nm^2/ms. The parameter a determines the absolute normalization of both curves whereas D determines the time scale of the decay. The absolute normalization has to take into account the limited efficiency of the cross-polarization steps and has been chosen to give the best fit of the experimental data to the theoretical curves. By changing the absolute normalization both values a and D change. As will be discussed below the determination of ξ_{het} is insensitive to the absolute normalization of the decay curves. The curves from the two-filter and the one-filter experiments relative to each other have been normalized according to the theoretical ratio of their plateau values. As compared to the one-filter experiment the two-filter experiment additionally decays to the selected part. Hence the ratio of the plateau values of the one- and the two-filter experiments approximately corresponds to $p = F_4^\infty$. Taking into account the details of the 4D-CP echo experiment deviations of the ratio of the plateau values from F_4^∞ occurs for small ξ_{het}. This effect is discussed in the Appendix. It does not influence the analysis of the experimental data because values for $t_{m2} \to 0$ are not accessible anyway and therefore the experimental curves cannot be normalized to $F_4^\xi(0) = 1$. For estimating the influence of the absolute normalization on the result for ξ_{het} model curves have been calculated for plateau values of the one-filter experiment between 0.1 (Fig. 6) and 0.6 (Fig. 7). Figure 7 shows the model curves corresponding to a plateau value of 0.6. Comparison to Fig. 6 shows that the range of correlation lengths that is compatible with the experimental data is quite insensitive to the choice of D and a because ξ_{het} mainly influences the time at which the plateau value is reached. For both sets of model curves the experimental results are compatible with correlation lengths between 2 and 4 nm. The data from the two-filter experiment show that the plateau value is not yet reached for $t_{m2} = 0.3$ ms but is definitely reached for $t_{m2} = 3$ ms. Therefore values of ξ_{het} smaller than 2 nm as well as larger than 4 nm can be excluded. The length scales accessible by this experiment are limited by the rate exchange processes which also lead to a decay of F_4^ξ. Correlation lengths of $\xi_{het} \geq 100$ nm cannot be distinguished from infinite ξ_{het}. Within the experimental uncertainty only correlation lengths smaller than 20 nm can be determined.

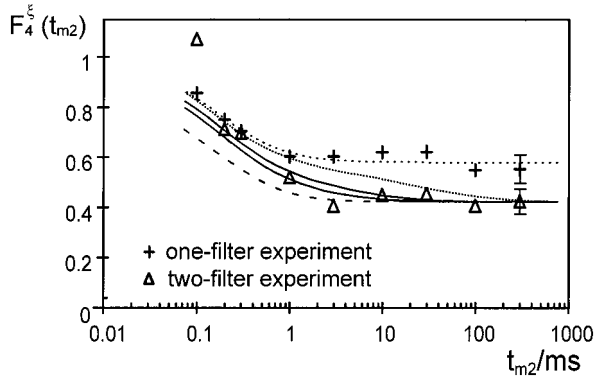

FIG. 7. Comparison of the same experimental data as shown in Fig. 6 to model calculations with $a = 0.2$ nm and $D = 0.19$ nm^2/ms. The different model curves correspond to the same length scales as those of Fig. 6.

The best fit to the experimental data especially for short t_{m2} has been achieved with $a = 0.1$ nm and $D = 0.42$ nm^2/ms. The value of a is a measure of the distance over which magnetization is transferred by the cross polarization. The small number is reasonable because a large loss of magnetization to the proton bath is compatible with the low signal-to-noise ratio of the 4D-CP echo experiment as compared to the 4D echo experiment. A larger value for a would correspond to cross polarization to a larger number of protons and consequently the observed poor signal-to-noise ratio would be solely due to inefficient cross polarization and not to a loss of magnetization to the proton bath. This assumption contradicts the results from the one-filter experiment. The decay of this curve shows that a loss of magnetization to the proton bath takes place. The corresponding diffusion coefficient $D = 0.42$ nm^2/ms is about a factor of 1.5 to 2 smaller than typical ^1H spin diffusion coefficients determined for polymers below their glass transition (*37*). This discrepancy can be attributed to the already mentioned scaling of the dipolar coupling by a factor of $-\frac{1}{2}$ during the spin lock pulses or to the dependence of D on the mobility.

DISCUSSION

By means of the new 4D-CP echo experiment the length scale of immobile regions in polyvinyl acetate has been determined to be $\xi_{het} = 3 \pm 1$ nm. This length corresponds to a cubic volume between 65 and 520 repeat units. It is not possible to infer further information about the shape of the immobile domains. They could be compact clusters as well as continuous interpenetrating structures. The result confirms theories that relate the dynamic properties in the glass transition range to a cooperativity length (*19*).

In contrast to previous experimental determinations of a characteristic length of the glass transition the NMR experi-

ment directly measures length scale and time scale of dynamic heterogeneities independently and without any external perturbations. Furthermore the length scale ξ_{het} has a well-defined meaning as expressed by Eq. [4]. The obtained value is comparable to results from the experiments that indirectly measure a cooperativity length (*16, 8*) as well as to the results obtained within the model of cooperatively rearranging regions (*19, 20*). The length scale ξ_{het} corresponds to the average diameter of immobile domains, whereas the typically studied length scale of cooperatively regions corresponds to the extension of mobile domains within the interpretation of Donth (*41*). For the present case of a selection of about 60% of the overall rate distribution the length scale ξ_{het} can be interpreted as an upper limit for the less well-defined cooperatively rearranging regions.

Further analysis of ξ_{het} as a function of temperature and of the filter time t_{m0} would be of interest. The temperature range that is accessible to this new exchange NMR experiment is rather limited because the mixing times have to be shorter than spin-lattice relaxation but the reorientation process has to be slow enough to justify the assumption that no dynamics take place during evolution and detection times and the rate exchange process has to be slower than the ^{1}H spin diffusion. The results from temperature dependent heat capacity spectroscopy interpreted within the model of cooperatively rearranging regions (*20*) indicate that no significant temperature dependence is to be expected in this range. By determining ξ_{het} for larger filter times t_{m0} the spatial distribution of segments correlated with their reorientation rates could be characterized. By selecting less segments with smaller reorientation rates the structure of the immobile domains could be studied as a function of the mobility of the selected segments. If the mobility depends on the size of a cooperatively rearranging region the length scale of the dynamic heterogeneities should increase with increasing filter strength. However, in order to achieve sufficient accuracy to detect any changes of the length scale the signal-to-noise ratio of the 4D-CP echo experiment has to be significantly improved. Please note that a 2D MAS version of the 3CP experiment was also developed (*42*).

SUMMARY

By combining static ^{13}C multidimensional exchange techniques with ^{1}H spin diffusion the 4D-CP echo experiment allows the direct determination of the length scale of dynamic heterogeneities. The well-defined correlation length corresponds to the average diameter of immobile domains. The experiment does not require external perturbation of the observed dynamics and the analysis does not rely on models about the nature of cooperative reorientations. The upper limit of accessible length scales is given by the rate exchange processes. In combination with the 4D echo experiment the new 4D-CP echo experiment yields detailed information about the dynamics in supercooled liquids. For polyvinyl acetate a length scale of $\xi_{het} = 3 \pm 1$ nm has been obtained. This result supports the concept of cooperative dynamics in the glass transition range.

APPENDIX

The complete theoretical description of the 4D-CP echo experiment assumes spin diffusion during t_{m2} as given by Eq. [2]. This equation can be rewritten as

$$\int\int \rho_{12}(\mathbf{r}_i)\, f(\mathbf{r}_j - \mathbf{r}_i)\rho_{34}(\mathbf{r}_j)d\mathbf{r}_i d\mathbf{r}_j \qquad [5]$$

with $\rho_{12}(\mathbf{r}) = \sum_k \cos((\omega_1 - \omega_2)t_p)\delta(\mathbf{r} - \mathbf{r}_k)$ and $\rho_{34}(\mathbf{r}) = \sum_k \cos(\omega_3 t_p) \cdot \cos(\omega_4 t_p)\delta(\mathbf{r} - \mathbf{r}_k)$ where the sum is over all ^{13}C spins. Qualitatively $\rho_{12}(\mathbf{r})$ and $\rho_{34}(\mathbf{r})$ are a measure of the density of slow ^{13}C nuclei. Furthermore the abbreviation $f(\mathbf{r}_j - \mathbf{r}_i) = \exp(-(\mathbf{r}_i(0) - \mathbf{r}_j(t_{m2}))^2/(4Dt_{m2}))$ is used. Substituting $\mathbf{r}_j$ by $(\mathbf{r}_j + \mathbf{r}_i)$ in Eq. [5] yields

$$\int\int \rho(\mathbf{r}_i)\, f(\mathbf{r}_j)\rho((\mathbf{r}_j + \mathbf{r}_i))d\mathbf{r}_i d\mathbf{r}_j. \qquad [6]$$

Thus the integration over $\mathbf{r}_i$ becomes independent of $f(\mathbf{r})$ and the integral can be replaced by an average density correlation defined as $\overline{\rho(\mathbf{r}_j)} = \int \rho(\mathbf{r}_j + \mathbf{r}_i)\rho(\mathbf{r}_i)d\mathbf{r}_i / \int \rho(\mathbf{r}_i)d\mathbf{r}_i$.

In general, in addition to spin diffusion rate exchange during t_{m2} has to be taken into account which results in a decrease of the density of immobile segments in the initially selected regions. Therefore, $\overline{\rho(\mathbf{r})} = \delta(\mathbf{r}) + \overline{\rho_0(\mathbf{r})}$ has to be replaced by a time dependent average density $\overline{\rho(\mathbf{r}, t_{m2})}$. The delta function is weighted with $F_4(t_{m2})$. The second term of $\rho_0(\mathbf{r})$, describing the increased probability of finding immobile ^{13}C atoms around the initially selected ^{13}C, has to be scaled by a function that accounts for the amount of slow rates that become fast and additionally for the amount of fast segments that become slow. For long times t_{m2} the density must still be given by p/ξ_0^3. Therefore the time dependent density $\rho_0(\mathbf{r}, t_{m2})$ is expressed by $(p + (1 - p)\exp(-2|\mathbf{r}_C|/\xi_{het})) \cdot y(t_{m2})$ with a function $y(t_{m2})$ that decays from 1 to 0 on the same time scale as F_4.

$$y(t_{m2}) = \frac{F_4(t_{m2}) - F_4^\infty}{1 - F_4^\infty} \qquad [7]$$

Finally the spatial distribution of magnetization during the cross-polarization sequences has to be considered. The transfer of magnetization from ^{13}C atoms to protons is accompanied by a spatial distribution around $\mathbf{r} = \mathbf{r}_C = 0$. This process can be interpreted as a preceding diffusion process resulting in a Gaussian distribution of magnetization with variance $a^2 = 2Dt_0$ and it can be taken into account by replacing the spin

diffusion time t_{m2} by an effective time $t_{\mathrm{eff}} = t_{m2} + t_0$. The Gaussian distribution of magnetization during the transfer back from ^{1}H to ^{13}C is modeled by weighting the average density of ^{13}C atoms $\overline{\rho(\mathbf{r}_C, t_{m2})}$ with the factor $\exp(-(\mathbf{r}-\mathbf{r}_C)^2/2a^2)$. The complete expression for $F_4^{\xi}(t_{m2})$ therefore reads

$$
\begin{aligned}
F_4^{\xi}(t_{m2}) \propto & \frac{1}{(4\pi D t_{\mathrm{eff}})^{3/2}} \int\int \exp\left(-\frac{\mathbf{r}^2}{4Dt_{\mathrm{eff}}}\right) \\
& \times \exp\left(-\frac{(\mathbf{r}-\mathbf{r}_C)^2}{2a^2}\right) \overline{\rho(\mathbf{r}_C, t_{m2})}\, d\mathbf{r}\, d\mathbf{r}_C \\
= & \frac{1}{(4\pi D t_{\mathrm{eff}})^{3/2}} \int \exp\left(-\frac{\mathbf{r}^2}{4Dt_{\mathrm{eff}}}\right) \\
& \times \left[\exp\left(-\frac{\mathbf{r}^2}{2a^2}\right) F_4(t_{m2}) + \frac{1}{\xi_0^3} \int \right. \\
& \exp\left(-\frac{(\mathbf{r}-\mathbf{r}_C)^2}{2a^2}\right) \left(p + (1-p) \right. \\
& \left. \left. \times \exp\left(-\frac{2|\mathbf{r}_C|}{\xi_{\mathrm{het}}}\right) y(t_{m2}) \right) d\mathbf{r}_C \right] d\mathbf{r} \qquad [8]
\end{aligned}
$$

with $p = F_4^{\infty}$. In the case of the one-filter experiment with $\rho_0(\mathbf{r}_C) = \xi_0^{-3}$ an analytical expression for F_4^{ξ} can be found because the integrals of the type $\int \exp(-\mathbf{r}^2/C)d\mathbf{r}$ can be represented by the solutions of the corresponding one-dimensional integrals. For $p \neq 1$ additionally an integral of the type $\int \exp(-(\mathbf{r}-\mathbf{r}_C)^2/2a^2)\exp(-2|\mathbf{r}_C|/\xi_{\mathrm{het}})d\mathbf{r}_C$ occurs which can be reduced to error functions and has been solved numerically in the present case. The plateau value $F_4^{\xi}(\infty)/F_4^{\xi}(0)$ for the one-filter experiment is given by

$$
\frac{(1/\xi_0^3(2\pi a^2)^{1.5})}{((1/2)^{1.5} + 1/\xi_0^3(2\pi a^2)^{1.5})}
$$

and for the two-filter experiment by

$$
\frac{p(1/\xi_0^3(2\pi a^2)^{1.5})}{(1/2)^{1.5} + p \cdot 1/\xi_0^3(2\pi a^2)^{1.5} + (1-p)\, f(\xi_{\mathrm{het}})}
$$

with the integral

$$
\begin{aligned}
f(\xi_{\mathrm{het}}) = & (4\pi D t_{\mathrm{eff}})^{-1.5} \int \exp\left(-\frac{\mathbf{r}^2}{4Dt}\right) 1/\xi_0^3 \int \\
& \times \exp\left(-\frac{(\mathbf{r}-\mathbf{r}_C)^2}{2a^2}\right)(1-p) \\
& \times \exp\left(-\frac{2\mathbf{r}_C}{\xi_{\mathrm{het}}}\right) d\mathbf{r}_C d\mathbf{r}.
\end{aligned}
$$

For $\xi_{\mathrm{het}} \gg a$ the ratio of the plateau values of the one-filter and the two-filter experiments approaches p whereas for smaller ξ_{het} it decreases.

ACKNOWLEDGMENTS

We thank K. Schmidt-Rohr for his contributions to the development of the pulse sequence, S. Reinsberg for valuable discussions, and H. Zimmermann for providing us with the ^{13}C enriched PVAc. U.T. gratefully acknowledges financial support from the BMBF and the Stiftung Stipendien-Fonds des Verbandes der Chemischen Industrie. This project was carried out within the Sonderforschungsbereich 262 Glaszustand und Glasübergang nichtmetallischer amorpher Materialien, Mainz, funded by the Deutsche Forschungsgemeinschaft.

REFERENCES

1. M. D. Ediger, C. A. Angell, and S. R. Nagel, *J. Phys. Chem.* **100,** 13200 (1996).
2. C. A. Angell, *Science* **267,** 1924 (1995).
3. K.-L. Li, A. A. Jones, P. T. Inglefield, and A. D. English, *Macromolecules* **22,** 4198 (1989).
4. W. Schnauss, F. Fujara, K. Hartmann, and H. Sillescu, *Chem. Phys. Lett.* **166,** 381 (1990).
5. K. Schmidt-Rohr and H. W. Spiess, *Phys. Rev. Lett.* **66,** 3020 (1991).
6. F. Fujara, B. Geil, H. Sillescu, and G. Fleischer, *Z. Phys. B-Condensed Matter* **88,** 195 (1992).
7. C. T. Moynihan and J. Schroeder, *J. Non-Cryst. Solids* **160,** 52 (1993).
8. M. T. Cicerone and M. D. Ediger, *J. Chem. Phys.* **103,** 5684 (1995).
9. A. Heuer, M. Wilhelm, H. Zimmermann, and H. W. Spiess, *Phys. Rev. Lett.* **75,** 2851 (1995).
10. R. Böhmer, G. Hinze, G. Diezemann, B. Geil, and H. Sillescu, *Europhys. Lett.* **36,** 55 (1996).
11. B. Schiener, R. Böhmer, A. Loidl, and R. V. Chamberlin, *Science* **274,** 752 (1996).
12. R. Richert, *J. Phys. Chem. B* **101,** 6323 (1997).
13. G. Adam and J. H. Gibbs, *J. Chem. Phys.* **43,** 139 (1965).
14. E. V. Russell, N. E. Israeloff, L. E. Walther, and H. A. Gomariz, *Phys. Rev. Lett.* **81,** 1461 (1998).
15. U. Tracht, M. Wilhelm, A. Heuer, H. Feng, K. Schmidt-Rohr, and H. W. Spiess, *Phys. Rev. Lett.* **81,** 2727 (1998).
16. R. Richert, *Phys. Rev. B* **54,** 15762 (1996).
17. M. Arndt, R. Stannarius, W. Gorbatschow, and F. Kremer, *Phys. Rev. E* **54,** 5377 (1996).
18. M. Arndt, R. Stannarius, H. Groothues, E. Hempel, and F. Kremer, *Phys. Rev. Lett.* **79,** 2077 (1997).
19. E. Donth, *J. Non-Cryst. Solids* **53,** 325 (1982).
20. J. Korus, E. Hempel, M. Beiner, S. Kahle, and E. Donth, *Acta Polym.* **48,** 369 (1997).
21. M. Foley and P. Harrowell, *J. Chem. Phys.* **98,** 5069 (1993).
22. S. C. Glotzer, N. Jan, T. Lookman, A. B. MacIsaac, and P. H. Poole, *Phys. Rev. E* **57,** 7350 (1998).
23. J. Jäckle, *Prog. Theor. Phys. Suppl.* **126,** 53 (1997).

24. C. Donati, S. C. Glotzer, P. H. Poole, W. Kob, and S. J. Plimpton, *Phys. Rev. Lett.* **80,** 2338 (1998).

25. K. Schmidt-Rohr and H. W. Spiess, "Multidimensional Solid-State NMR and Polymers," Academic Press, London (1994).

26. M. Vogel and E. Rössler, *J. Phys. Chem. A* **102,** 2102 (1998).

27. S. C. Kuebler, A. Heuer, and H. W. Spiess, *Phys. Rev. E* **56,** 741 (1997).

28. A. Heuer, S. C. Kuebler, U. Tracht, H. W. Spiess, and K. Okun, *in* "Structure and Dynamics of Glasses and Glass Formers" (C. A. Angell, K. L. Ngai, J. Kieffer, T. Egami, and G. U. Nienhaus, Eds.), MRS Symposia Proceedings No. 455, Materials Research Society, Pittsburgh (1997).

29. G. Hinze, *Phys. Rev. E* **57,** 2010 (1998).

30. G. Hinze, R. Böhmer, G. Diezemann, and H. Sillescu, *J. Magn. Reson.* **131,** 218 (1998).

31. R. Böhmer, G. Diezemann, G. Hinze, and H. Sillescu, *J. Chem. Phys.* **108,** 890 (1998).

32. R. Böhmer, R. V. Chamberlin, G. Diezemann, B. Geil, A. Heuer, G. Hinze, S. C. Kuebler, R. Richert, B. Schiener, H. Sillescu, H. W. Spiess, U. Tracht, and M. Wilhelm, *J. Non-Cryst. Solids* **235–237,** 1 (1998).

33. A. Döß, G. Hinze, G. Diezemann, R. Böhmer, and H. Sillescu, *Acta Polym.* **49,** 56 (1998).

34. U. Tracht, A. Heuer, and H. W. Spiess, *J. Non-Cryst. Solids* **235–237,** 27 (1998).

35. A. Heuer, *Phys. Rev. E* **56,** 730 (1997).

36. J. Crank, "The Mathematics of Diffusion," 2nd ed., Clarendon Press, Oxford (1975).

37. J. Clauss, K. Schmidt-Rohr, and H. W. Spiess, *Acta Polym.* **44,** 1 (1993).

38. F. Mellinger, M. Wilhelm, and H. W. Spiess, *Macromolecules,* submitted.

39. S. Zhang, B. H. Meier, and R. R. Ernst, *Solid State Nucl. Magn. Reson.* **1,** 313 (1992).

40. K. Zemke, K. Schmidt-Rohr, and H. W. Spiess, *Acta Polym.* **45,** 148 (1994).

41. E. Donth, *J. Polym. Sci., B: Polym. Phys.* **34,** 2881 (1996).

42. M. Wilhelm, H. Feng, U. Tracht, and H. W. Spiess, *J. Magn. Reson.* **134,** 255 (1998).